Photoluminescence Hot Paper

International Edition: DOI: 10.1002/anie.201700436
German Edition: DOI: 10.1002/ange.201700436

Transition-Metal-Doped NIR-Emitting Silicon Nanocrystals

Sourov Chandra, Yoshitake Masuda, Naoto Shirahata, and Françoise M. Winnik**

Abstract: *Impurity-doping in nanocrystals significantly affects their electronic properties and diversifies their applications. Herein, we report the synthesis of transition metal (Mn, Ni, Co, Cu)-doped oleophilic silicon nanocrystals (SiNCs) through hydrolysis/polymerization of triethoxysilane with acidic aqueous metal salt solutions, followed by thermal disproportionation of the resulting gel into a doped-Si/SiO_2 composite that, upon HF etching and hydrosilylation with 1-n-octadecene, produces free-standing octadecyl-capped doped SiNCs (diameter ≈ 3 to 8 nm; dopant < 0.2 atom %). Metal-doping triggers a red-shift of the SiNC photoluminescence (PL) of up to 270 nm, while maintaining high PL quantum yield (26 % for Co doping).*

Silicon has played an important role throughout the evolution of mankind, from the sharp silica flints that became man's first tools, to building materials, ceramics, and more recently integrated circuits and solar cells. Beyond bulk silicon, silicon nanocrystals (SiNCs) and silicon quantum dots, discovered by Brus in 1992,[1] are actively pursued in view of their size- and surface-dependent optical properties, and low toxicity, coupled with the high natural abundance of Si. Current research trends focus on the preparation of doped silicon nanocrystals, in which the dopant brings a new property to the SiNCs. For instance, doping SiNCs with boron, a p-dopant, or phosphorous, an n-dopant, enables the formation of p–n junctions between B- and P-doped SiNCs, an important achievement in the area of solar cells.[2] Metal-doped NCs have not been explored extensively so far, although they could act as non-toxic multimodal contrast agents in medical imaging, replacing the currently available metal-doped CdSe and ZnSe QDs.[3,4] To date, metal-doped SiNCs were obtained through a multistep procedure starting from Fe- or Mn-doped alkali silicides,[5] and through hydride reduction of a mixture of silicon tetrachloride and a metal halide.[6] The latter process led to SiNCs doped with approximately 0.5 % transition metal, which emit blue to green light. The transition metal-doped SiNCs reported herein incorporate no more than 0.2 % transition metal atoms, yet emit with absolute photoluminescence quantum yields (PL QY) as high as 26 % within the red-to-NIR spectral region. This achievement is important as it leads the way to plurimodal medical imaging agents responsive to light within the biological window as well as to other fields addressable by transition metals.

Unlike the previous preparations of metal-doped SiNCs,[7,8] the reported synthesis starts with the hydrolysis/polymerization of triethoxysilane (TES) in the presence of an acidic metal salt aqueous solution. The resulting $(HSiO_{1.5})_n$ gel[9] loaded with metal ions is subjected to thermal disproportionation, HF-etching and hydrosilylation with octadecene, yielding free-standing metal-doped SiNCs (Figure 1). A

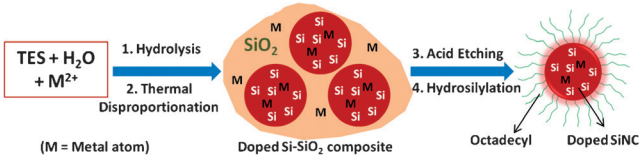

Figure 1. Representation of the preparation of octadecyl-capped metal-doped silicon nanocrystals, starting from triethoxysilane (TES).

related approach was used previously to prepare from blue-[10] to red-to-NIR-emitting SiNCs of high PL QY and outstanding photostability.[9] This method was redesigned to modulate favorably the competition between Si–Si and Si–metal bond formation in the disproportionation step to secure adequate doping yields. The metal ions concentration was kept very low to increase the probability of forming the mixed metal/Si nuclei necessary to initiate crystallization. If the dopant concentration is too high, the strain caused by dopant-host incompatibility prevents the nucleation of metal-doped SiNCs.

The synthesis was carried out with Ni^{2+}, Mn^{2+}, Co^{2+}, Cu^{2+}, and no added metal salt (Supporting Information). The first step, hydrolysis/polymerization of TES, was performed by adding aqueous salt solutions of increasing concentration to a fixed volume of TES (10 mL, 90 mM). This yielded colorful

[*] Dr. S. Chandra, Dr. N. Shirahata, Prof. F. M. Winnik
WPI International Centre for Nanoarchitectonics (MANA)
National Institute for Materials science (NIMS)
1-1 Namiki, Tsukuba 305-0044 (Japan)
E-mail: SHIRAHATA.Naoto@nims.go.jp
Dr. Y. Masuda
National Institute of Advanced Industrial Science and Technology (AIST)
Shimoshidami, Moriyama, Nagoya (Japan)
Prof. F. M. Winnik
Departement de Chimie, Universite de Montreal
CP 6128 Succursale Centre Ville, Montreal QC H3C 3J7 (Canada)
and
Department of Chemistry and Faculty of Pharmacy
University of Helsinki
00014 Helsinki (Finland)
E-mail: francoise.winnik@umontreal.ca
Supporting information and the ORCID identification number(s) for the author(s) of this article can be found under: http://dx.doi.org/10.1002/anie.201700436.

Table 1: Size of SiNCs embedded in SiO_2 matrix and free-standing SiNCs as a function of metal concentration (M = Ni, Mn, Co, and Cu).[a]

	Metal ions							
MCl_2	$NiCl_2$		$MnCl_2$		$CoCl_2$		$CuCl_2$	
[mg]	d_{co} [nm]	d_{fs} [nm]	d_{co} [nm]	d_{fs} [nm]	d_{co} [nm]	d_{fs} [nm]	d_{co} [nm]	d_{fs} [nm]
0	5.5	4.8	–	–	–	–	–	–
6.25	6.3	–	6.4	–	–	–	–	–
12.5	7.5	7.2	7.5	6.9	6.1	6.0	4.4	–
25	8.6	–	9.3	–	8.0	–	3.1	–
50	15.9	–	51.6	–	–	–	–	–
100	25.5	–	59.0	–	–	–	–	–

d_{co} = Avg. diameter of SiNC embedded in SiO_2 matrix (measured by XRD); d_{fs} = Avg. diameter of free-standing SiNC (measured by XRD); [a] Amount of TES = 90 mM (10 mL); "–" refers no doping of SiNCs.

$(HSiO_{1.5})_n$ gels (Table 1 and the Supporting Information, Figure S1). The gels were dried and subjected to thermal disproportionation under vacuum, either at 1100 °C for 2 h or at 900 °C for 6 h. X-ray diffraction (XRD) patterns of the doped and undoped Si/SiO_2 composites prepared in the presence of metal salt (0.10 ± 0.01 mM) and without salt and heated at 1100 °C are shown in Figure 2a. The patterns show a broad signal centered at $2\theta = 21.5°$, characteristic of SiO_2 (orange dot) and sharp signals at $2\theta = 28°$, 47°, and 56° (blue dots), corresponding to the [111], [220], and [311] lattice planes of crystalline silicon.[11] Small peaks, also attributed to the SiNCs, appear at $2\theta = 69°$ [400], 76° [331], and 88° [422]. These peaks are more prominent in the XRD patterns of doped samples compared to those of the SiNCs.[12] The ratio of the intensity of the XRD signals at 21.5° and 28.0° (Supporting Information, Figure S2) is higher in Co-, Ni- and Mn-doped Si–SiO_2 composites compared to that of the undoped composite. The ratio recorded for Cu-doped Si–SiO_2 is very low and the diameter of the SiNC domains is very small as well, which indicates that Cu interferes with Si crystallization (Table 1). The Si:SiO_2 ratio and the size of the Si domains depend on the initial metal salt concentration (Figure 2b, Table 1, and the Supporting Information, Figure S3). The particle size increases with increasing initial metal ions concentration (Supporting Information, Figure S4).

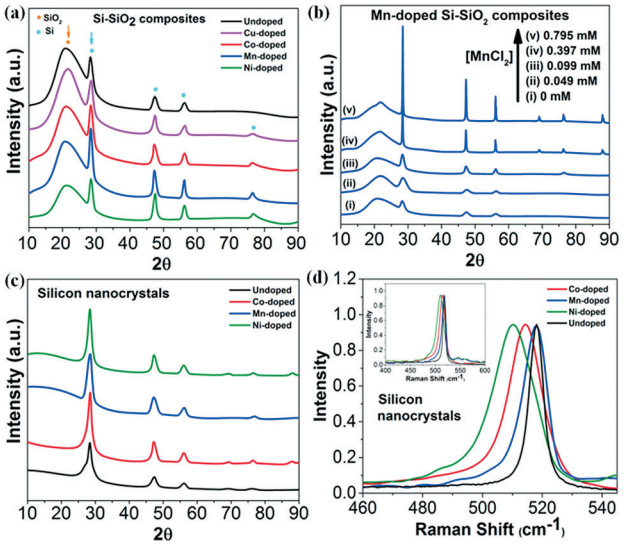

Figure 2. X-ray diffraction patterns of the materials grown at 1100 °C. a) Si–SiO_2 composites with and without dopant, b) Mn-doped Si–SiO_2 composites obtained with different starting concentrations of $MnCl_2$ and c) free-standing doped and undoped SiNCs. d) Raman spectra of the free-standing SiNCs grown from Si–SiO_2 composites at 1100 °C (inset: full Raman spectra).

The crystallization and growth of SiNCs within the silica matrix are controlled primarily by the temperature and duration of the thermal treatment of $(HSiO_{1.5})_n$;[13] that is, the diameter of the SiNCs embedded in the SiO_2 matrix increases with processing temperature and duration. The XRD pattern (Supporting Information, Figure S5) of a composite grown at 900 °C for 6 h presents weak broad peaks at 28.6° and 47.8°, assigned to the [111] and [220] lattice planes of silicon, and a strong broad peak at 22.6° that is attributed to the amorphous silica matrix, indicating the presence of small SiNCs inside the SiO_2 matrix. Composites recovered after a 2 h treatment of $(HSiO_{1.5})_n$ gels at 900 °C consist of amorphous SiO_2 devoid of SiNCs, as indicated by the XRD pattern.

Next, the SiO_2 matrix surrounding the doped-SiNCs was removed by HF etching, immediately followed by hydrosilylation with octadecene and centrifugation, which yielded stable octadecyl-capped SiNCs. XRD patterns of the metal-doped SiNCs, shown in Figure 2c, confirm the formation of native crystalline SiNCs and the absence of SiO_2. The Raman spectra of Ni-, Co-, and Mn-doped and undoped SiNCs display bands at 510, 518, 518, and 520 cm^{-1}, respectively (Figure 2d). The shifts to lower wavenumbers upon metal doping,[14] reflect the strain or distortion of the silicon lattice caused by the presence of dopant atoms.[15]

The metal-doped SiNCs, as determined by transmission electron microscopy (TEM), are larger than the SiNCs, and their size distribution is narrower. The diameter of NPs grown at 1100 °C ranges from 7.3 ± 1.3 nm (Co) and 7.5 ± 1.5 nm (Mn) to 8.75 ± 3.25 nm (Ni), compared to 5.0 ± 2.5 nm in the case of undoped SiNCs (Figure 3). The size of nanocrystals grown at 900 °C follows similar trends (Supporting Information, Figure S6), which reflects the effect of the dopant on crystal nucleation and growth.[16] The dopant atom concentration within doped SiNCs was determined by inductively coupled plasma optical emission spectroscopy (ICP-OES).[4,17] Doped SiNCs grown at 1100 °C contain 0.11% Mn, 0.07% Co, and 0.18% Ni, whereas doped samples obtained at 900 °C contain 0.14% Mn and 0.10% Co. The X-ray photoelectron spectroscopy (XPS) spectrum recorded for Co-doped SiNCs (Supporting Information, Figure S7) presents a small signal at circa 778.5 eV, which is attributed to $Co2p_{3/2}$ electron and gives further support to the presence of Co^0 in the SiNCs. The estimated Co/Si atom ratio (0.075) is in good agreement with the value obtained from the ICP-OES analysis of the same sample.

Key photophysical properties of the metal-doped SiNCs, summarized graphically in Figure 4b, are presented below, focusing on samples grown at 1100 °C. Like SiNCs,[9] metal-doped SiNCs absorb light over the entire UV range, with a weak tail in the visible range (Figure 4a, left axis). Their PL

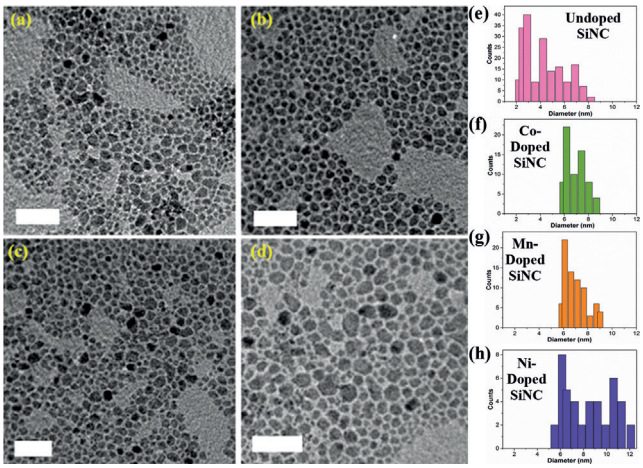

Figure 3. TEM images of a) undoped, b) Co-doped, c) Mn-doped, and d) Ni-doped SiNCs, grown at 1100 °C (scale bars = 50 nm). e–h) Size-distribution histograms of the corresponding doped and undoped SiNCs.

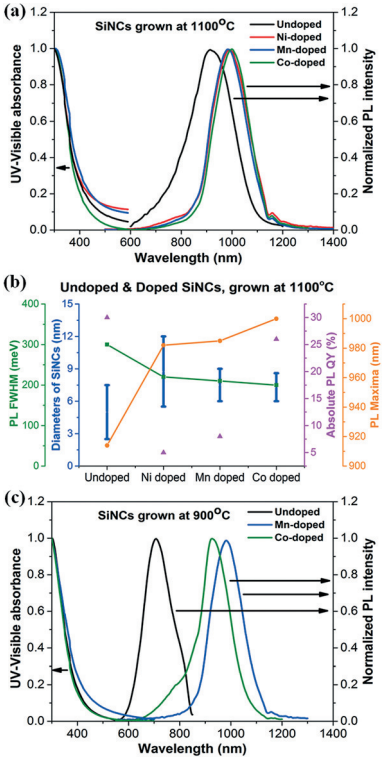

Figure 4. UV/visible absorbance and PL spectrum of SiNCs, grown at a) 1100 °C and c) 900 °C. b) Particle-size distribution and optical properties of doped and undoped SiNCs, grown at 1100 °C.

spectra exhibit narrow emission bands, centered at 985, 992, and 1000 nm for Mn, Ni, and Co, respectively, which correspond to red-shifts of 67, 74, and 82 nm, compared to the emission of SiNC (918 nm) (Figure 4 a,b). While red shifts of PL bands are closely associated with changes in the diameter of the crystals,[5,18,19] these phenomena are also related to the occurrence of radiative recombination of excitons from trap states in silicon nanocrystals.[7] In addition, the FWHM of the emission band of the doped SiNCs is narrower than that of the original SiNCs (Figure 4 b and the Supporting Information, Table S1), an effect attributed to the narrower size distribution of the metal-doped NCs. As seen in Figure 3 e–f, the original SiNC sample contains a significant fraction of NCs diameter (d) of $2 < d < 5$ nm (blue-shifted PL). The size distributions of all metal-doped NC samples are narrower than in the case of SiNCs and display an insignificant fraction of NCs with diameters in the 1–5 nm range.

The absolute PL quantum yield (QY) of doped SiNCs, determined by the standardized integrating-sphere method, (see the Supporting Information) is significantly lower than that of SiNCs (QY 30 %) in the case of Mn- (QY = 8 %) and Ni-doped SiNCs (QY = 5 %), whereas Co-doping hardly affects the nanocrystals PL QY (26 %). We tentatively attribute this effect to the generation of nonradiative pathways in doped SiNCs induced by the energy levels of the inserted Mn and Ni atoms. The fact that Co insertion hardly affects the QY of SiNCs may indicate that the energy levels of Co are such that they do not affect the SiNC emissive pathways. The absorption and emission spectra of doped SiNCs grown at 900 °C follow the same trends, compared to undoped SiNCs (Figure 4 c). The PL spectra of Mn- and Co-doped SiNCs have maxima at 984 and 928 nm, respectively, showing a remarkable circa 270 nm red shift, compared to SiNCs ($\lambda_{em} = 706$ nm). The corresponding FWHM and QYs are listed in the Supporting Information, Table S2.

For a mechanistic interpretation of the doped SiNCs photophysical characteristics, we assume that the metal atoms within the silicon lattice in doped SiNCs create stable impurity states in close vicinity of the valence band (VB).[20,21] Upon excitation, electrons flow from the VB to the conduction band (CB) absorbing exactly the same energy of light as the energy needed to excite SiNCs. The position of the impurity (or trap) state in between the VB and CB varies depending on the electronic configurations of the metal atoms. Hence, one expects that the position of the trap states will vary with the composition and size of the host SiNCs, as reflected by the dopant-dependence of the PL spectra. Compared to the PLE spectrum of SiNCs (Supporting Information, Figure S8), which decreases monotonically in intensity from 300 nm to approximately 480 nm, the PLE spectra of doped SiNCs feature a weak but distinct band centered around 365 nm. This band is seen in the PLE spectra of all doped SiNCs, irrespective of the dopant and the NC growth temperature; although the overall band patterns of the PLE spectra vary depending on the dopants.[6,18,22]

The PL decay of metal-doped SiNCs follows a bi-exponential profile (Supporting Information, Figure S9). The decay is slower than that of SiNCs, in which the slow component of the decay has a lifetime of circa 515 μs. Co-doped SiNCs grown at 1100 °C have the longest lifetime, with a slow component that exhibits a lifetime of approximately 1236 μs (see the Supporting Information, Tables S3 and S4). By displacing a few Si atoms from their crystal lattice, the metal atoms decrease the number of donor states, which results in the increase of the PL lifetime observed experimentally.[23] Undoped SiNCs grown at 900 °C show an exceptionally short PL lifetime, compared to all the other SiNCs described, which may be related to the poor crystal-

linity of SiNCs grown at 900 °C, which facilitates nonradiative decay through defects and shortens the PL lifetime.[24]

In summary, we have described a new synthesis of metal-doped SiNCs that enabled us to prepare the first near-IR-emitting metal-doped SiNCs. We monitored the effects of the synthesis parameters and the dopant nature and composition on the structural and photophysical properties of doped-SiNCs. Because organophilic nanocrystals, such as the doped SiNCs prepared, can be converted into stable water-dispersible nanoparticles through known interfacial transfer processes,[9] this study leads the way towards bimodal medical imaging agents of low toxicity and strong emission in the biological window.

Acknowledgements

This study was supported by the WPI-Program and NIMS Molecule & Material Synthesis Platform in "Nanotechnology Platform Project" both operated by the Ministry of Education, Culture, Sports, Science and Technology (MEXT), Japan. N.S. thanks financial supports from the JST A-step (AS282I006e), Kakenhi (26390024) and Sumitomo Foundation.

Conflict of interest

The authors declare no conflict of interest.

Keywords: doping · nanocrystals · photoluminescence · silicon · thermal disproportionation

How to cite: *Angew. Chem. Int. Ed.* **2017**, *56*, 6157–6160
Angew. Chem. **2017**, *129*, 6253–6256

[1] K. A. Littau, P. J. Szajowski, A. J. Muller, A. R. Kortan, L. E. Brus, *J. Phys. Chem.* **1993**, *97*, 1224–1230.
[2] B. L. Oliva-Chatelain, T. M. Ticich, A. R. Barron, *Nanoscale* **2016**, *8*, 1733–1745.
[3] D. J. Norris, A. L. Efros, S. C. Erwin, *Science* **2008**, *319*, 1776–1779.
[4] S. C. Erwin, L. Zu, M. I. Haftel, A. L. Efros, T. A. Kennedy, D. J. Norris, *Nature* **2005**, *436*, 91–94.
[5] X. Zhang, M. Brynda, R. D. Britt, E. C. Carroll, D. S. Larsen, A. Y. Louie, S. M. Kauzlarich, *J. Am. Chem. Soc.* **2007**, *129*, 10668–10669.
[6] B. F. P. McVey, J. Butkus, J. E. Halpert, J. M. Hodgkiss, R. D. Tilley, *J. Phys. Chem. Lett.* **2015**, *6*, 1573–1576.
[7] M. Dasog, J. Kehrle, B. Rieger, J. G. C. Veinot, *Angew. Chem. Int. Ed.* **2016**, *55*, 2322–2339; *Angew. Chem.* **2016**, *128*, 2366–2384.
[8] H. Sugimoto, M. Fujii, K. Imakita, *Nanoscale* **2014**, *6*, 12354–12359.
[9] S. Chandra, B. Ghosh, G. Beaune, U. Nagarajan, T. Yasui, Y. Baba, N. Shirahata, F. M. Winnik, *Nanoscale* **2016**, *8*, 9009–9019.
[10] S. Chandra, G. Beaune, N. Shirahata, F. M. Winnik, *J. Mater. Chem. B* **2017**, *5*, 1363–1370.
[11] B. Ghosh, Y. Masuda, Y. Wakayama, Y. Imanaka, J. Inoue, K. Hashi, K. Deguchi, H. Yamada, Y. Sakka, S. Ohki, T. Shimizu, N. Shirahata, *Adv. Funct. Mater.* **2014**, *24*, 7151–7160.
[12] M. Dasog, Z. Yang, J. G. C. Veinot, *CrystEngComm* **2012**, *14*, 7576–7578.
[13] E. J. Henderson, J. A. Kelly, J. G. C. Veinot, *Chem. Mater.* **2009**, *21*, 5426–5434.
[14] P. Miska, M. Dossot, T. D. Nguyen, M. Grun, H. Rinnert, M. Vergnat, B. Humbert, *J. Phys. Chem. C* **2010**, *114*, 17344–17349.
[15] a) K. M. Hanif, R. W. Meulenberg, G. F. Strouse, *J. Am. Chem. Soc.* **2002**, *124*, 11495–11502; b) D. C. Dillen, K. M. Varahramyan, C. M. Corbet, E. Tutuc, *Phys. Rev. B* **2012**, *86*, 045311.
[16] A. K. Guria, N. Pradhan, *Chem. Mater.* **2016**, *28*, 5224–5237.
[17] X. D. Pi, R. Gresback, R. W. Liptak, S. A. Campbell, U. Kortshagen, *Appl. Phys. Lett.* **2008**, *92*, 123102.
[18] H. Sugimoto, M. Fujii, K. Imakita, S. Hayashi, K. Akamatsu, *J. Phys. Chem. C* **2013**, *117*, 11850–11857.
[19] C. M. Hessel, D. Reid, M. G. Panthani, M. R. Rasch, B. W. Goodfellow, J. Wei, H. Fujii, V. Akhavan, B. A. Korgel, *Chem. Mater.* **2012**, *24*, 393–401.
[20] P. Wu, X. P. Yan, *Chem. Soc. Rev.* **2013**, *42*, 5489–5521.
[21] D. S. Bohle, C. J. Spina, *J. Phys. Chem. C* **2010**, *114*, 18139–18145.
[22] V. Proshchenko, Y. Dahnovsky, *J. Phys. Chem. C* **2014**, *118*, 28314–28321.
[23] J. Luo, S. Zhao, P. Wu, K. Zhang, C. Peng, S. Zheng, *J. Mater. Chem. C* **2015**, *3*, 3391–3398.
[24] B. Ghosh, M. Takeguchi, J. Nakamura, Y. Nemoto, T. Hamaoka, S. Chandra, N. Shirahata, *Sci. Rep.* **2016**, *6*, 36951.

Manuscript received: January 13, 2017
Final Article published: April 7, 2017

